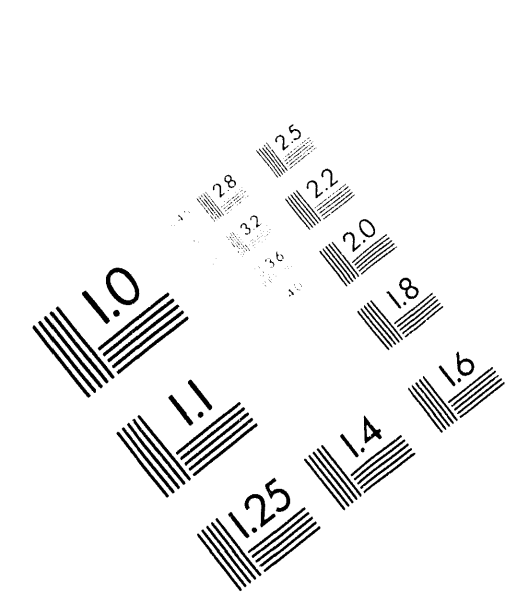

Association for Information and Image Management

1100 Wayne Avenue, Suite 1100
Silver Spring, Maryland 20910

301/587-8202

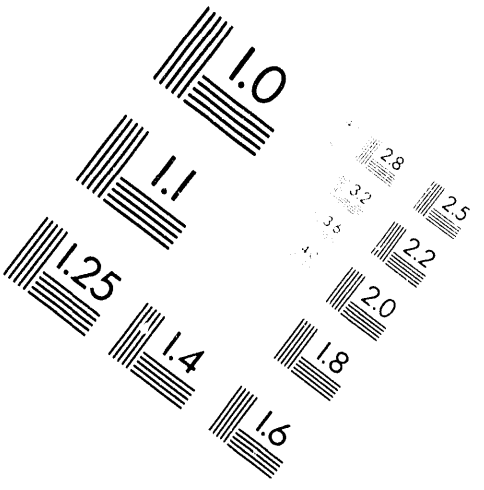

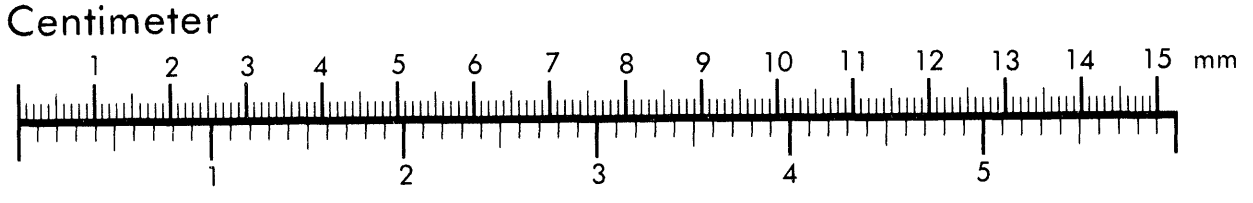

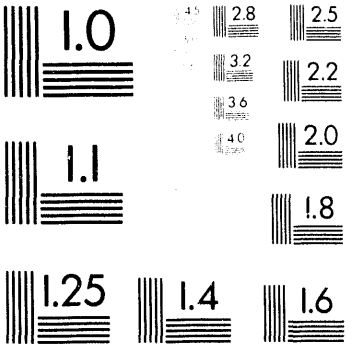

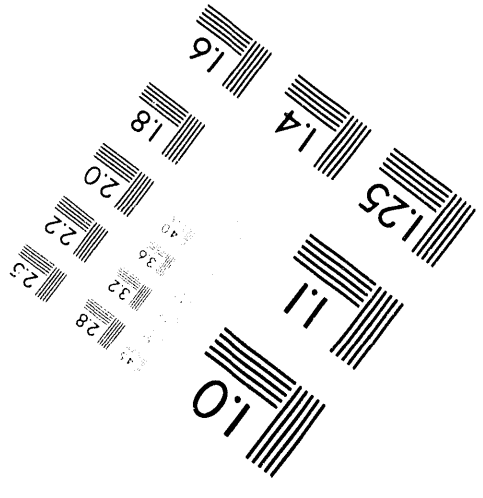

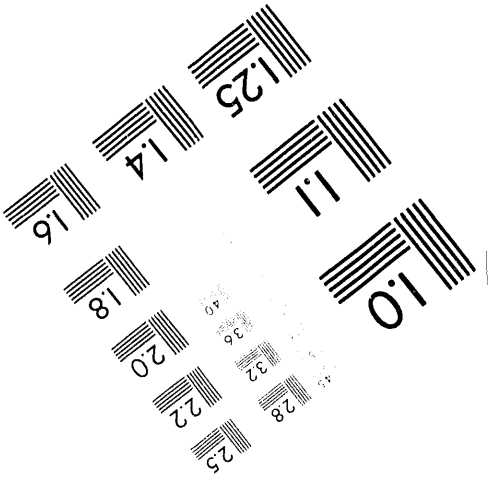

MANUFACTURED TO AIIM STANDARDS
BY APPLIED IMAGE, INC.

1 of 1

SAND93-1320
Unlimited Release
Printed May, 1993

Distribution
Category UC-706

Modeling of the Second Stage of the STAR 1.125 Inch Two-Stage Gas Gun†

Donald B. Longcope, Jr.
Structural Dynamics Department, 1434
Sandia National Laboratories
Albuquerque, New Mexico 87185

Abstract

The second stage of the Shock Technology and Applied Research (STAR) facility two-stage light gas gun at Sandia National Laboratories has been modeled to better assess its safety during operation and to determine the significance of various parameters to its performance. The piston motion and loading of the acceleration reservoir (AR), the structural response of the AR, and the projectile motion are determined. The piston is represented as an incompressible fluid while the AR is modeled with the ABAQUS finite element structural analysis code. Model results are compared with a measured profile of AR diameter growth for a test at maximum conditions and with projectile exit velocities for a group of tests. Changes in the piston density and in the break diaphragm opening pressure are shown to significantly affect the AR loading and the projectile final velocity.

---

†. This work, conducted at Sandia National Laboratories, was supported by the U. D. Department of Energy under Contract No. DE-AC04-94AL85000

Acknowledgements

The author thanks Clint Hall, Department 1433, for helpful discussions regarding the operation of the two-stage gas gun and comparisons between modeling and test results; Mike Forrestal, Department 9723, for suggesting the incompressible fluid model of the piston deforming in the acceleration reservoir; and Phil Stanton, Department 1433, for suggesting that the H_2 kinetic energy be accounted for.

Table of Contents

Figures

Tables

Modeling of the Second Stage of the STAR 1.125 Inch Two-Stage Gas Gun

Introduction

The second stage operation of the STAR facility 1.125 in. bore two-stage gas gun has been modeled in order to better assess its safety by understanding the structural response of its most highly loaded component, the transition section, or acceleration reservoir (AR), and to better understand the significance of the operating parameters to its performance. The gun operation is unusual for high-pressure equipment because on maximum performance shots the AR typically experiences a small amount of permanent deformation which requires monitoring and results in limited service life. Under these extreme operating conditions it is especially important to understand the AR response in a maximum performance shot.

During operation of the gun, Fig. 1, propellant in the breech accelerates the piston in the pump tube. As it travels down the pump tube, the piston compresses the H_2 gas. When the front of the piston nears the tapered section of the AR, the burst diaphragm opens and the H_2 gas begins to accelerate the projectile in the launch tube. In the tapered section of the AR, the front of the piston accelerates compressing the H_2 gas to high pressure, which accelerates the projectile. The piston front stops a few inches into the launch tube and the volume of H_2 gas begins to expand in the launch tube while continuing to accelerate the projectile.

A model is developed for the piston loading of the AR and the projectile motion. The piston is represented as an unsteady, incompressible fluid at typical pressures which are much greater than its strength; the H_2 gas is compressed adiabatically with high-pressure effects included; and the projectile is a rigid mass. The coupled piston/projectile model is solved numerically and the transient piston pressure is applied to an ABAQUS finite element model of the AR. The analytical results are correlated with AR diameter growth in a test at maximum conditions and with projectile exit velocity in a group of tests. A factor of safety for the piston velocity in one high-performance test is calculated. Changes in operating parameters are indicated which would reduce the AR loading and increase the projectile final velocity.

Piston Deformation and Projectile Motion

As the piston enters the tapered region of the AR it is severely deformed and loads the inner AR surface with a high, dynamic pressure. The piston motion is coupled to the compression of the H_2 gas and the motion of the projectile. The AR is assumed rigid for the purpose of determining the piston pressure on it.

Piston Deformation. In the converging region of the AR, the piston is idealized as an unsteady, incompressible fluid composed of polyethylene and teflon portions, Fig. 2. This is justified by the fact that the significant pressures on the AR are of the order of 150,000 psi, or higher, while the yield strengths of the piston materials are of the order of 3,000 psi, Refs. [2,3]. The yield strengths of both materials are pressure and rate dependent, Refs. [3,4], but the increases due to these effects are not significant compared to the pressures in the AR. The dimensions of the AR and piston are given in Figs. 3 and 4.

Results were developed using the continuity equation, Ref. [5] ,

$$A\dot{x} = \text{constant} \tag{1}$$

for an incompressible fluid and the Bernoulli or energy equation

$$\rho\frac{\dot{x}^2}{2} + P + \int_0^s \frac{\partial \dot{x}}{\partial t} ds = \text{constant} \tag{2}$$

for unsteady, incompressible flow in a straight pipe with no elevation change, where the integration is along a streamline of the flow. In Eqs(1,2), A is the cross-sectional area of the flow, $\dot{x}$ is the flow velocity in the direction of motion (s>0), ρ is the density, P is the pressure, and t is time. Applying Eqs.(1,2) to the portion of the piston in the pump tube (s<0) gives

$$\ddot{x}_2 = -\left(\frac{P_2 - P_1}{M}\right)A_2, (s < 0) \tag{3}$$

where M is the mass of the piston in s<0, 1 refers to the back surface of the piston, and 2 is the beginning of the tapered region. According to Eq(1), all piston particles in the pump tube have the same velocity. When the front of the piston is in the tapered region, applying Eqs(1,2) to the portion of the piston in this region gives

$$P_2 = P_3 + \frac{\rho}{2}\left(\frac{r_2^4}{r_3^4} - 1\right)\dot{x}_2^2 + \frac{\rho r_2 s_3}{r_3}\ddot{x}_2, (0 < s_3 < s_e) \tag{4}$$

where 3 refers to the front surface of the piston and ρ is the density of the polyethylene. For the particular piston geometry, the teflon/polyethylene interface does not enter the tapered region until the piston front reaches the exit of this region.

When the piston exits the tapered region, it is assumed to be in a region of constant radius equal to the radius of the launch tube. For this portion of the piston,

$$P_e = P_3 + \rho\,(s_3 - s_e)\,\ddot{x}_e,\ (s_3 > s_e) \tag{5}$$

It is assumed that at the same time as the piston front reaches the exit, the polyethylene/ teflon interface is entering the tapered region (this a close approximation). When the interface is in the tapered region, the use of Eqs(1,2) gives

$$P_i = P_e + \frac{\rho}{2}\left(\frac{r_2^4}{r_e^4} - \frac{r_2^4}{r_i^4}\right)\dot{x}_2^2 + \frac{(s_e - s_i)\,r_2^2}{r_3 r_i}\ddot{x}_2,\ (0 < s_i < s < s_e) \tag{6}$$

and an equation, for $0<s<s_i$, which is obtained by replacing subscript 3 with i in Eq(4).

H_2 Compression. When the piston is at the breech, just before firing, the pump tube and AR are filled with H_2 gas at 134 psig. As the piston travels down the pump, the H_2 gas is compressed and when the piston reaches a position approximately 4.5 in. from the entrance to the AR tapered section, the break diaphragm opens, Ref. [7]. This is the time at which the present modeling begins. The H_2 gas is assumed to expand instantly into the small additional volume between the break diaphragm and the projectile. The H_2 is compressed and the pressure increases as the piston motion reduces the initial volume faster than the projectile increases it during its early motion. Eventually the projectile velocity becomes great enough that the H_2 volume begins to increase and the pressure reaches a maximum. A typical H_2 pressure range is from 10,000 psi to 150,000 psi. The compression of the H_2 is assumed to be adiabatic and quasistatic. It is represented by the PANDA equation of state data, Ref. [6] , which includes high pressure effects, such as dissociation. Over the pressure range of interest this data gives a pressure 20 to 45 per cent higher than that for an ideal gas. In the numerical procedure used to determine the piston and projectile motion, it is convenient to fit this data with an analytic function. The function used is a relation which holds for the adiabatic compression of an ideal gas,

$$\frac{P_3}{P_0} = \left(\frac{V_0}{V_3}\right)^k \tag{7}$$

where 0 refers to the initial state and 3 to a subsequent state. The parameter k is chosen to best fit the PANDA data and for the calculated results values of 1.75 and 1.68 were used.

Projectile Motion. The projectile is modeled simply as a rigid mass with the equation

$$m\ddot{y} = A_e P_3 \tag{8}$$

where y is the displacement of the projectile. m is its mass, and P_3 is the H_2 pressure. Friction between the projectile and launch tube walls is neglected.

Solution Procedure. When the piston front is in the tapered region, the coupled piston/ projectile motion is described by Eqs.(3,4,7,8). These equations are nonlinear and the quantities P_2, M, P_3, r_3, s_3, and V_3 are functions of time. P_1 is taken to be a constant, since the volume of the pump tube is large compared to the volume change resulting from piston motion in the AR. A standard numerical procedure is used to determine the pressure, piston motion, and projectile motion. The initial piston position and velocity are known and the initial projectile position and velocity are zero. Using these values in the equations determines all the other dependent variables at t=0. In this process it is convenient to substitute for $\ddot{x}_2$ in Eq.(4) using Eq.(3). Values of quantities at $t=\Delta t$, where Δt is a small increment of time, are determined from values of their derivatives at t=0 by extrapolation and the process is repeated to continue the solution. When the piston front has exited the tapered region and the polyethylene/teflon interface has entered it, the additional equations (5,6) apply and the conditions of continuity of pressure and flow velocity at the interface are used.

Results for Test 3 Conditions. Test 3 was the third of a series of tests performed to break in a new AR. Tests 1 and 2 produced only elastic and incipient plastic responses, but test three was at near maximum charge and produced a nominally maximum AR diameter growth of 0.010 in. The piston velocity was 25,300 in./s (0.643 km/s) when the piston front was 4.5 in. from the beginning of the tapered section of the AR, as determined by velocity pin measurement, and the break diaphragm opened at this time, as inferred from projectile launch tube velocity measurements, Ref. [7] . These are the initial conditions for the calculation of piston and projectile motion. The break diaphragm opening pressure was taken to be 17,600 psi. This is the result of a calculation of the adiabatic compression of the H_2, using the data of Ref. [6] , from an initial pressure of 134 psig when the piston was at the breech. The break diaphragm was designed to open at a static pressure of 10,000 psi, but no test results of this are known. The values of the input parameters used in the calculation are:

$\dot{x}_2(0)$=25,300 in./s (0.643 km/s)

$s_3(0)$=-4.5 in.

$M(0)=15.0\ lb_m$ (6810 gm)

m=0.0634 lbm (28.8 gm)

$P_b=P_3(0)$ =17,600 psi

r_2=1.75 in.

r_e=0.55 in.

s_e=17.5 in.

ρ=8.60x10^{-5} lb-s^2-in.$^{-4}$ (0.92 gm/cm^3)

ρ_t=2.24x10^{-4} lb-s^2-in.$^{-4}$ (2.40 gm/cm^3)

$y(0)=\dot{y}(0)=0$

P_1=1,700 psi

k=1.75

This value of k fits Eq.(7) to the EOS data of Ref. [6] over the range 16,000 to 230,000 psi with a maximum error or 6%.

For the Test 3 conditions, Eqs.(3-8) were solved numerically giving the results shown in Figs. 5,6,7 for the projectile position, velocity, and acceleration; in Fig. 8 for the H_2 pressure; and in Figs. 9,10 for the piston front surface and back surface velocities. No measurements of these quantities were made in this test. These results span a range of projectile motion to near maximum velocity at a distance traveled of about 2/3 the length of the launch tube. The piston front surface velocity increases very rapidly in the AR and the back surface velocity decreases, but not nearly as rapidly. The peak front surface velocity occurs at the time the front reaches the exit of the tapered region and the abrupt drop to zero occurs a short time later when the exit pressure drops to zero.

Pressure histories at the axial locations, s=0,5,10, and 15 in., in the AR are shown in Fig 11. The maximum pressure is 400,000 psi which is about twice the static pressure to cause the AR hoop strain to reach the material ultimate of 0.13; however the highly dynamic nature of the pressure actually produces much lower plastic strains. The abrupt drop to zero of the pressure histories at a time shortly after the peaks are reached corresponds to the AR exit (located at s=17.5 in.) pressure becoming zero. The pressure actually falls through zero, Fig. 12, and becomes tensile. The interpretation is that separation of the fluid piston occurs at this time. The sharpness of the pressure decrease suggests that even if material strength, which is a few thousand psi, were included in the model, separation would still occur. In typical maximum performance shots, pieces of the piston material are found near the launch tube entrance and the furthest the piston is found in the launch tube is about 10 inches from the entrance. In Test 3, at the time the pressure at the exit becomes zero, the piston front is about 2 inches beyond. This is the time t* at which the piston motion and pressure are set to zero and the piston modeling stops. The projectile motion and H_2 pressure decrease are allowed to continue. At t* the pressures have already fallen substantially below their maxima and to continue modeling beyond this point would require considering multiple material separations, the asymmetries associated with the ruptured diaphragm, and the expansion of the piston material into the cavity between the break diaphragm and the launch tube.

AR Structural Response

Structural Model. The inside surface of the tapered portion of the AR is loaded by the dynamic pressure determined from the piston deformation model. The response of the AR is represented by an ABAQUS, Ref. [8] , axisymmetric structural model composed of CAX4R elements, Fig. 13. When the AR is assembled into the gas gun, it is placed in compression by the beast and beast nut, Fig. 1. The compression causes the ring seals in the grooves at either end of the AR to deform and seal properly. Compressive forces transmitted through the seals restrain the ends of the AR at these locations, but the contact and restraint over the flat surfaces of the ends is uncertain. Fixed boundary conditions (zero axial and radial displacement) were chosen at the ends of the model. To bound the uncertainty, results for fixed and free end conditions were compared and permanent hoop strains were only a few per cent greater for the free end case. This indicates that uncertainty in the end restraints is not significant for the particular piston dynamic loading and response considered.

Specification of Stress-Strain Behavior of 4340 Steel. The objective of the structural model is to calculate the AR diameter growth for a typical maximum performance shot. Measurements, Ref. [7] , indicate the permanent hoop strain at the outside AR surface is of the order 0.1% and calculations indicate this corresponds to a permanent strain of about 1% at the inside surface. The AR is made of 4340 steel and the emphasis is on representing its behavior in this relatively small plastic strain range, rather than over its entire strain range which extends to an ultimate strain of 13%.

The strength of 4340 steel can vary by a factor of several, depending on the heat treatment. The stress-strain curve for the steel of the AR used in the later test comparisons was not measured, but the Rockwell C hardness was determined to be 39/40 at several locations, Ref. [9] . Using the data of Fig. 14 from Ref. [10] , this determines a tensile strength of 190,000 psi with an uncertainty of perhaps 10 per cent. According to the data given in Ref. [11] , the corresponding yield strength is about 7 per cent lower which is 177,000 psi. Fig. 15 from Ref. [12] shows the strain hardening in a 4340 steel of a strength comparable to that of the AR material. As the plastic strain increases, most of the hardening has occurred when the plastic strain reaches 1%. The hardening model is chosen to be isotropic with a linear increase from the yield strength to the ultimate strength at 1% plastic strain and constant thereafter to an ultimate strain of 13%, Ref. [11] . Fig. 15 also indicates that, above yield, the uniaxial compressive stress is about 10% higher than the tensile stress. Since both tensile and compressive hoop stresses of the order of the yield stress occur in the AR, a single stress-strain curve with yield and ultimate stresses 5 per cent higher than the above values is chosen to represent an average of the tensile and compressive behavior. This curve is used in the ABAQUS response model and is specified, Table 1, by an initial yield stress of 186,000 psi, linear strain hardening to an ultimate stress of 200,000 psi at 1% plastic strain, and finally constant stress to an ultimate plastic strain of 13%.

Response and Diameter Growth in Test 3. An approximation to the loading shown in Fig. 11 is applied to the AR finite element model of Fig. 13. The approximation is to apply the pressure at the s=5 in. location uniformly over the tapered region of the AR. The peak AR hoop strains are found to occur in the neighborhood of this point and the approximation is satisfactory elsewhere. The ABAQUS explicit solution procedure is chosen because of the highly dynamic nature of the loading. For the simple structural model, results are obtained in about 60 sec. of Cray YMP cpu time. Overall equivalent plastic strain contours are shown in Fig. 16 and a detail in the area of maximum hoop strain is shown in Fig. 17. These represent the plastic strain accumulated during the loading and show that it is a maximum at about one-third the AR length from the aft end. Fig. 18 shows the maximum permanent radial displacement at the inside surface is 0.023 in. at 8.35 in. from the aft end (node 91). This displacement is obtained by averaging the elastic oscillatory response at late time. The corresponding diameter increase is 0.046 in. (46 mils). The peak permanent radial displacement at the outside surface, Fig. 19, is at 7.38 in. from the aft end (node 102). The average is 0.006 in. and the diameter growth is 12 mils. Calculated values of diameter growth are compared with measured values, Ref. [7], in Fig. 20. The agreement in location of diameter growth is good and in magnitude is satisfactory, though the calculated values are generally larger. Additional calculations using a yield stress and ultimate stress 10% greater than those in Table 1, which are the maximum values within the uncertainty of these quantities, gave a maximum diameter growth of 10 mils.

AR loading and response were also calculated for P_b=10,000 psi, which is the nominal design pressure for the break diaphragm to open, and the same other Test 3 conditions. This gave significantly higher loading and AR diameter growth which was about twice as high that as shown in Fig. 20. For this value of P_b, the data of Ref. [6] was fitted using k=1.68 over the range 6,000 psi to 160,000 psi with an error of 6%.

Factor of Safety for Test 3. Additional AR response calculations with P_b =17,600 psi were performed to determine a factor of safety for the piston velocity in Test 3. The factor of safety specifies the piston velocity at which a rupture through the AR wall would occur. Failure is assumed to occur when the calculated equivalent plastic strain (PEEQ) exceeds 0.13, which is the ultimate uniaxial strain for the 4340 steel. When the piston velocity is 0.772 km/s, which is 1.2 times its Test 3 velocity, results of the model show a small localized region of failure near the inner AR surface. The location of this region is approximately where the maximum PEEQ is shown in Fig. 16. When the piston velocity is 0.965 km/s or 1.5 times its Test 3 velocity, the calculated region of failure is much larger and extends through 80% of the AR wall. The plasticity model of this calculation does not account for a reduction in material strength after failure, which, if included, would result in a larger failure region.

To account for the substantial decrease in material strength after failure, additional calculations were performed with the plasticity model modified to include softening by specifying that for PEEQ greater than 0.13, the Mises stress decreases linearly from 200,000 psi at PEEQ=0.13 to 20,000 psi at PEEQ=0.15 and then is constant for PEEQ>0.15. Calculations with this model showed that a piston velocity of 1.5 times its Test 3 velocity would produce failure through the entire AR wall over a substantial axial distance and that a piston velocity of 1.3 times its Test 3 velocity would cause failure

through only about 50% of the wall thickness. These results bound the factor of safety (FS) for the piston velocity, 1.3<FS<1.5, where FS is the ratio of the piston velocity to cause a rupture through the AR wall to the piston velocity of Test 3.

Projectile Exit Velocities

Projectile launch tube exit velocities were measured in several tests, Ref. [7] , for different piston velocities and projectile masses, Table 2. Calculated exit velocities are compared for the two plausible values of the diaphragm break pressure, discussed previously. Calculated velocities were obtained by estimating the asymptote from curves such as that of Fig. 6. The calculated velocities show reasonable agreement at the higher velocities, but all are higher than the measured velocities. The velocities for Pb=10,000 psi show better agreement than the velocities for Pb=17,600 psi. The model neglects friction between the projectile and launch tube wall. This is supported by the expectation that the projectile material in contact with the launch tube melted during early motion, Ref. [7] .

The model neglects the increases in kinetic energy of the H_2 gas as it is compressed in the AR and expands in the launch tube. At the suggestion of Ref. [13], the effect of this on the projectile final velocity was considered. Since the mass of the H_2 is 43.7g and its velocity near the projectile is the same as that of the projectile, the kinetic energies are comparable. The major portion of the kinetic energy increase of the H_2 occurs as it expands in the launch tube. This is accounted for by equating the increase in the kinetic energy of the projectile (with the H_2 kinetic energy neglected) to the sum of the kinetic energy increases of the H_2 gas and the projectile, during the time period from when the piston stops, t=t*, to when the projectile exits the launch tube. This gives the following equation for the corrected projectile final velocity, $\dot{y}_f^c$,

$$\dot{y}_f^c = \left[\frac{1 + \frac{\phi^2 m_H}{4m}}{1 + \frac{m_H}{4m}} \right]^{1/2} \dot{y}_f \qquad (9)$$

$$\phi = \frac{\dot{y}^*}{\dot{y}_f}$$

where $\dot{y}_f$ is the projectile final velocity (with H_2 kinetic energy neglected), $\dot{y}^*$ is the projectile velocity when the piston stops (t=t*), and m_H is the mass of the H_2 gas. In the development of this equation, the kinetic energy of the H_2 is approximated by assuming that all the H_2 is moving at an average velocity equal to one-half the projectile velocity. All the projectile final velocities of Table 2 are corrected in this manner. Corrected projectile final velocities, $\dot{y}_f^c$, are given in Table 2 and show improved agreement with the measured values. All the corrected velocities for P_b =10,000 psi are within 3% of the measured velocities, with the exception of the low velocity of Test 1.

Improvement of Gun Performance

The effect of changing the piston material on the AR loading was considered. For the conditions of Test 3, AR loading and projectile motion were calculated, assuming an all-teflon piston of the same mass as the actual piston. The AR loading at the axial station, s=5 in., is compared for the actual and all-teflon pistons in Fig. 21. The actual piston is designated 'polyethylene' because only the front 8 in. long polyethylene portion affects the AR loading. This is because the volume of the tapered cavity of the AR is approximately equal to the volume of this polyethylene portion and the pressure drops to zero very shortly after the teflon portion enters the tapered region. For the teflon piston, the peak pressure and that portion of the impulse under the curve which affects the dynamic response (above the 170,000 psi pressure level) are considerably lower than for the polyethylene piston. Fig. 22 shows that the projectile exit velocity for the all-teflon piston is only a few per cent lower than that for the polyethylene piston. Since the piston model is an incompressible fluid, the only difference in the materials is in their densities which are 2.40 gm/cm^3 and 0.92 gm/cm^3 for the teflon and polyethylene, respectively.

The magnitude of the break diaphragm pressure has a significant effect on both the AR loading and on the projectile final velocity. Increasing the break pressure increases the projectile final velocity and decreases the loading on the AR. The effect on projectile velocity is indicated in Table 2. When the break pressure is 17,600 psi, the peak pressure and impulse on the AR are about 30% lower than when the break pressure is 10,000 psi.

Conclusions and Recommendations

Within the uncertainty of specification of model parameters, the model results show satisfactory agreement with measurements of AR diameter growth and projectile exit velocities for maximum performance shots. Calculations indicate the factor of safety (FS) for the piston velocity in Test 3, a typical high-performance test, was bounded by $1.3<FS<1.5$. The model indicates that the AR loading can be decreased or, for the same loading, the projectile final velocity can be increased by increasing the density of the piston material or by increasing the break diaphragm pressure.

Recommendations for tests which would allow better evaluation of the model are:

- Measure the rupture pressure of the nominally 10,000 psi break diaphragm currently in use.
- Measure the velocity of the projectile in the gun barrel with a visar technique to obtain a velocity-time curve, which includes the initial motion.
- Make laboratory stress-strain measurements of the particular 4340 steel of which a new AR is made in addition to obtaining Rockwell C hardness data.

Better definition of the model could allow a reasonable estimate of the plastic strain which accumulates in successive maximum performance shots and a possible prediction of the AR life. Because of hardening of the steel, it is expected that the additional plastic strain and diameter growth on maximum shots after the first will be much smaller than on the first shot.

References

[1]Operation Manual for a Converted Two-Stage Light-Gas Research Gun, Contract No. 16-8060 with Sandia Corp., Delco Electronics, Santa Barbara, Ca, Dec., 1971.

[2]"1974 Materials Selector," Materials Engineering, Vol. 78, No. 4, Sept., 1973.

[3]D. R. Mears, K. D. Pae, and J. A. Sauer, "Effects of Hydrostatic Pressure on the Mechanical Behavior of Polyethylene and Polypropylene," Journal of Applied Physics, Vol. 40, No. 11, Oct. 1969, pp 4229-4237.

[4]J. Harding, "The Effect of High Strain Rate on Material Properties," Materials at High Strain Rates, edited by T. Z. Blazynski, Elsevier Applied Science Publishers Ltd, London, 1987.

[5]W. Kaufman, Fluid Mechanics, Mcgraw-Hill Book Co., Inc., 1963.

[6]Gerald I. Kerley, "CTH Reference Manual: The Equation of State Package," SAND91-0344, Sandia National Laboratories, Albuquerque, NM, May, 1991.

[7]Clint, Hall, private communication, Dept. 1433, Sandia National Laboratories, Albuquerque, NM, March, 1993.

[8] "ABAQUS User's Manual,", Version 4.8, Hibbett, Karlsson, Sorensen, Inc., Providence, R. I., 1989.

[9]Herb Webster, 'Certification of Rockwell C Hardness Data for Two Acceleration Reservoirs," Phoenix Heat Treating Co., Phoenix, AZ, May, 1990.

[10]Structural Alloys Handbook, 1985 Ed., Vol. 1, Metals and Ceramics Information Center, Batelle's Columbus Laboratories, Columbus, Ohio.

[11]Modern steels and Their Properties, Bethlehem Steel Corp., 6th Ed., 1966.

[12]Howard E. Boyer, editor, Atlas of Stress-Strain Curves, ASM International, Metals Park, Ohio, 1987, p. 211.

[13]Phil Stanton, private communication, Department 1433, Sandia National Laboratories, Albuquerque, NM, May, 1993.

Table 1. Uniaxial Plastic Behavior of 4340 Steel

Plastic Strain	Yield Stress (psi)
0.0	186,000
0.010	200,000
0.13	200,000

Table 2. Measured and Calculated Projectile Velocities

Test No.	Piston Vel. (km/s)	Proj. Mass (gm)	Proj. Vel. (km/s)	Calc. Proj. Vel. (km/s) Pb=17,600 psi initial	Pb=17,600 psi corr.	Pb=10,000 psi initial	Pb=10,000 psi corr.
1	.342	21.6	4.0	6.9	6.2	5.7	5.2
2	.494	21.4	5.67	7.6	6.9	6.5	5.9
3	.643	28.8	----	7.8	7.2	6.6	6.1
4	.626	34.4	5.83	7.2	6.7	6.2	5.8
5	.626	32.2	5.91	7.4	6.9	6.2	5.8
6	.625	24.6	6.44	8.1	7.4	6.9	6.3
7	.63	14.7	6.9	9.7	8.6	8.0	7.1

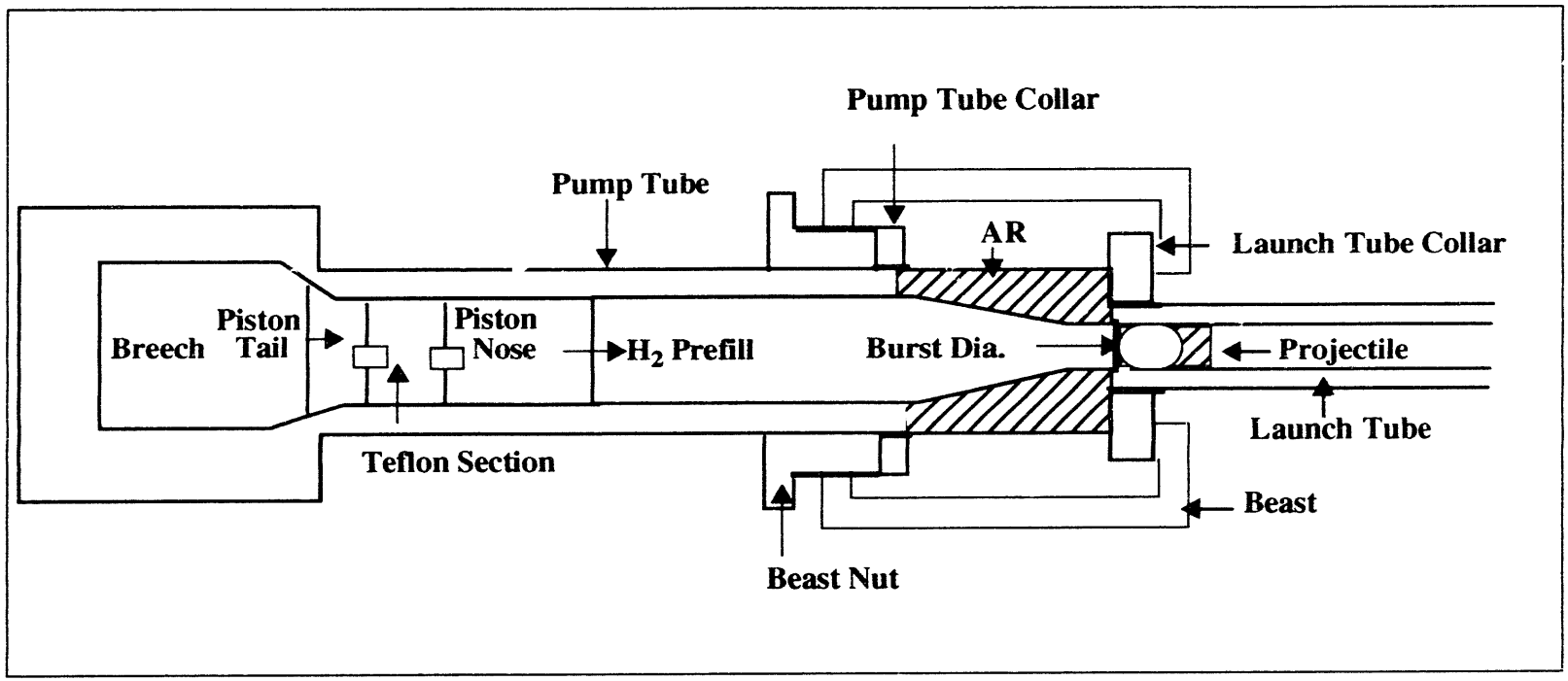

Figure 1. Sketch of STAR 1.125 Inch Bore Two-Stage Gas Gun

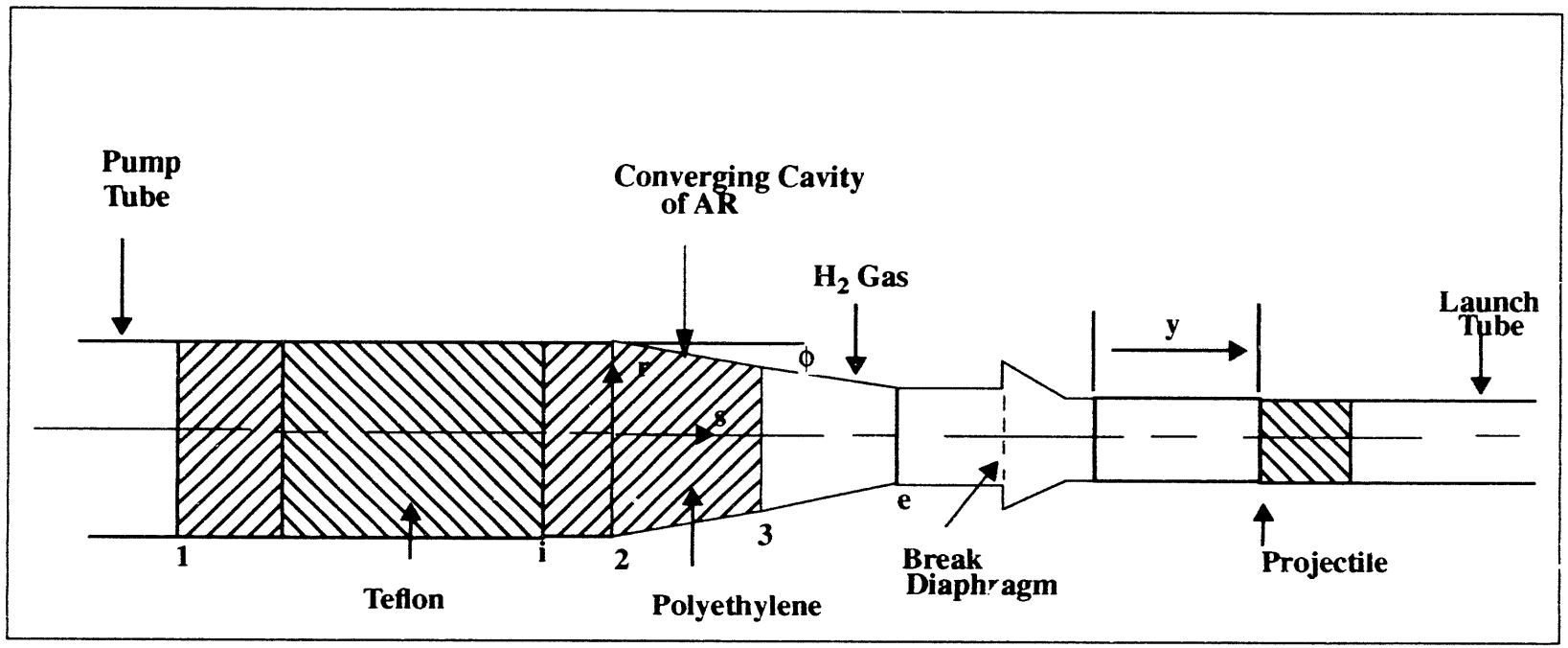

Figure 2. Geometry of Piston/H_2/Projectile Model

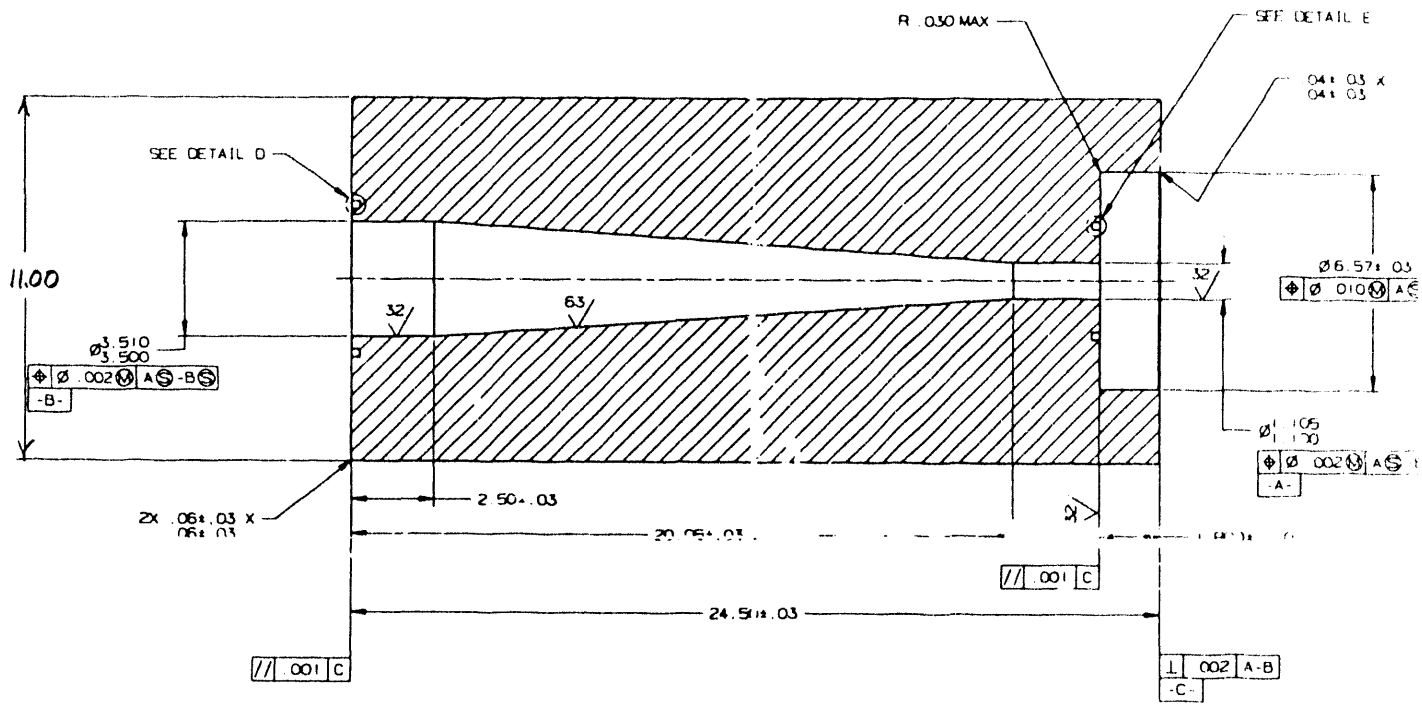

Figure 3. AR Geometry

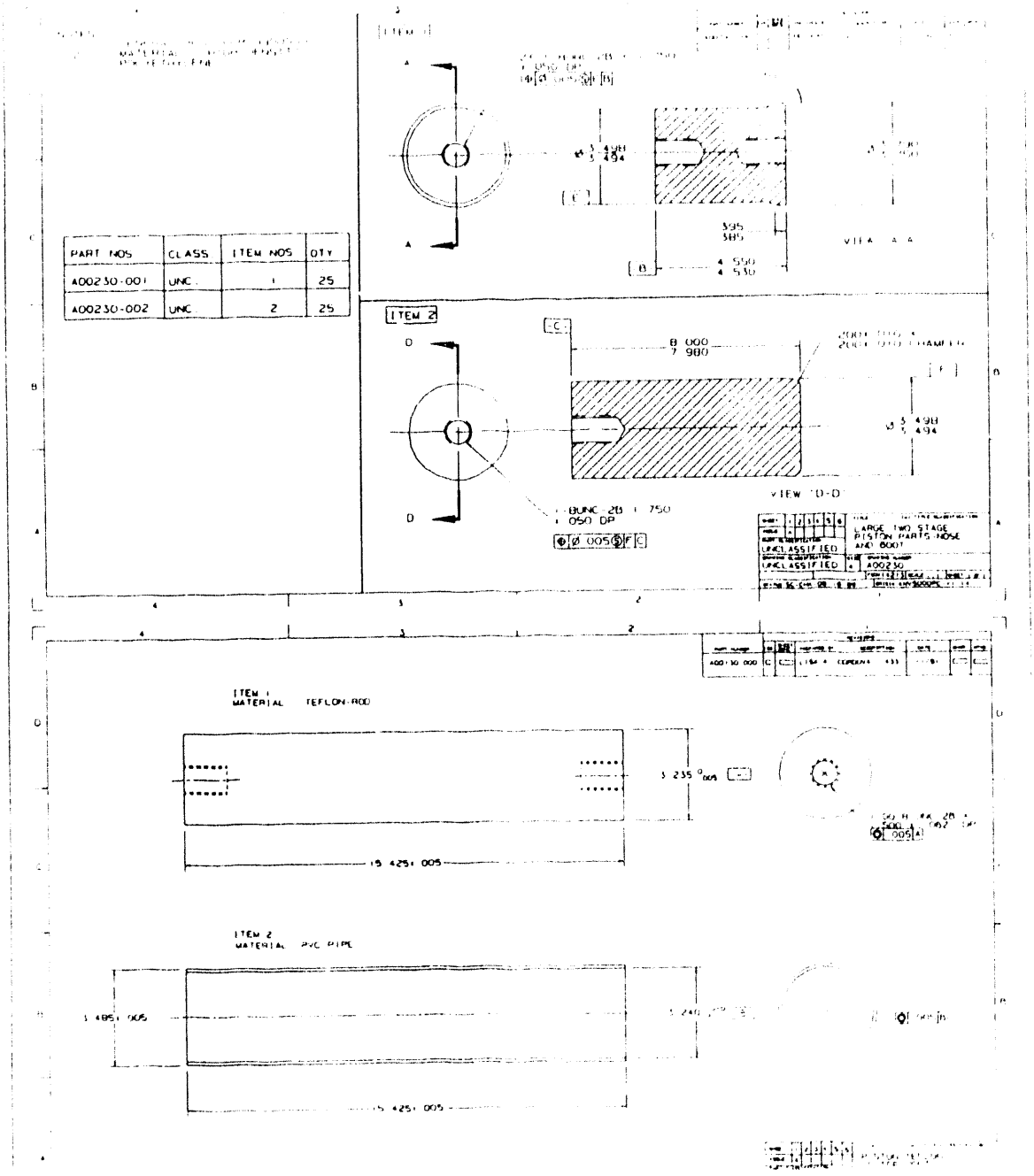

Figure 4. Geometry of Polyethyene/Teflon Piston

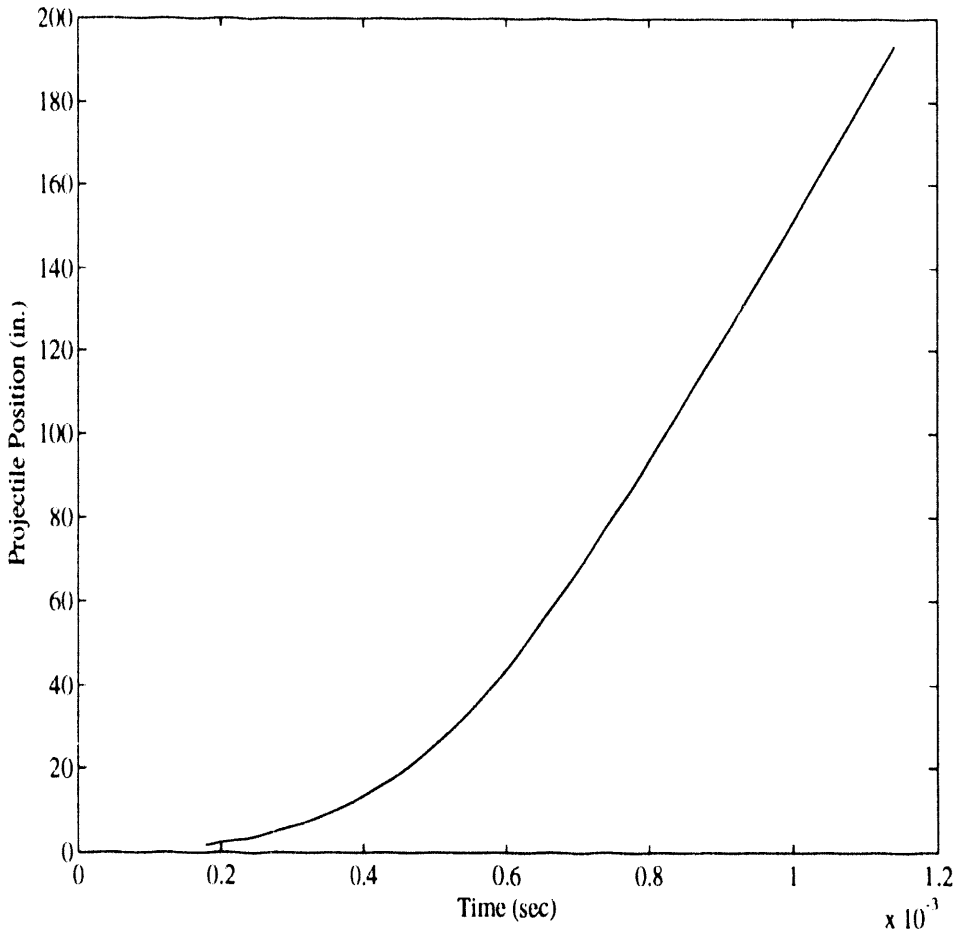

Figure 5. Projectile Position in Test 3

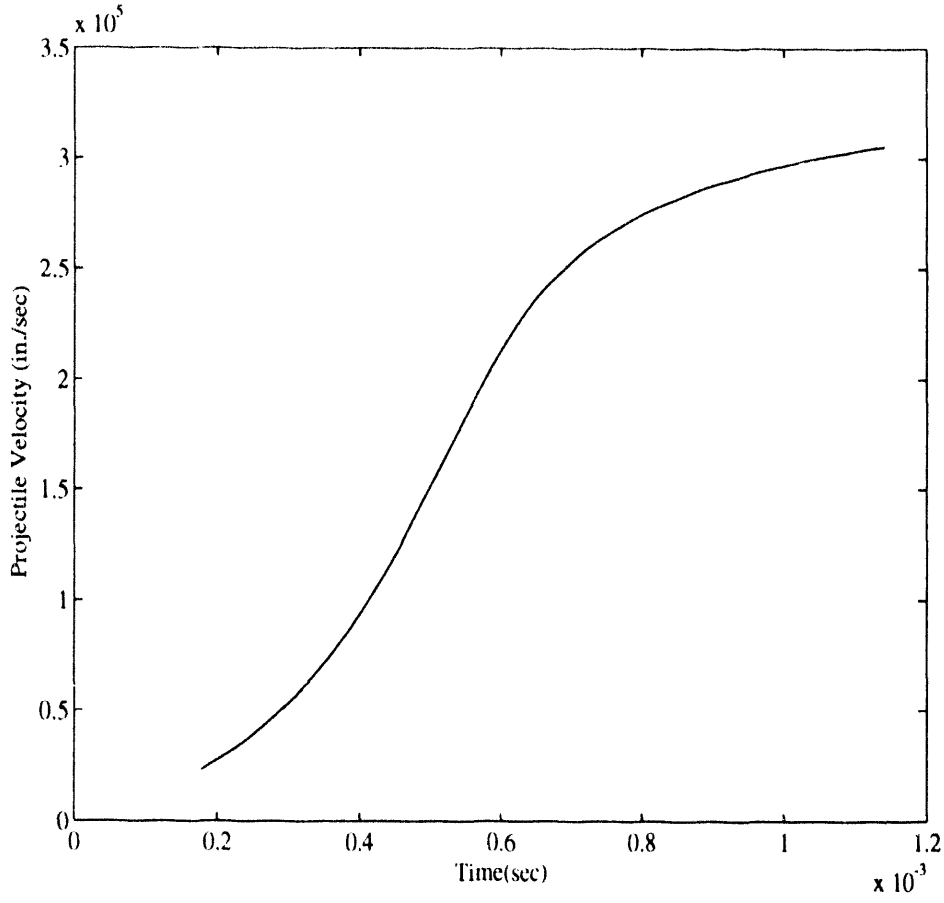

Figure 6. Projectile Velocity in Test 3

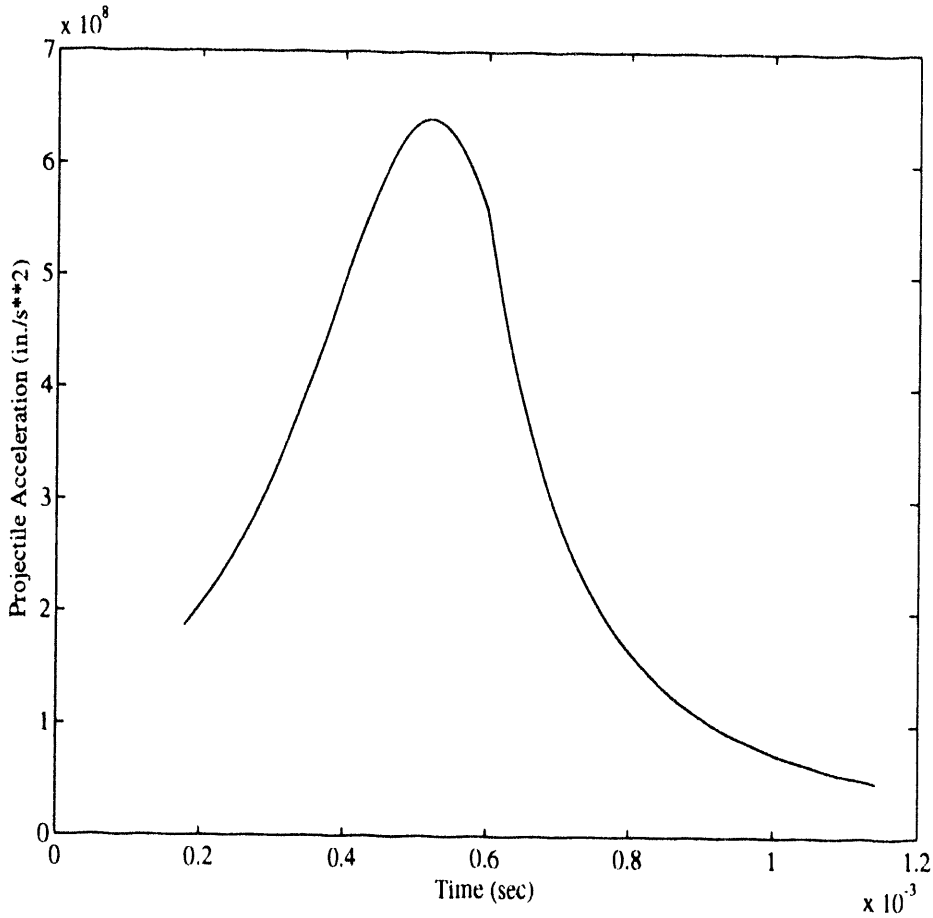

Figure 7. Projectile Acceleration in Test 3

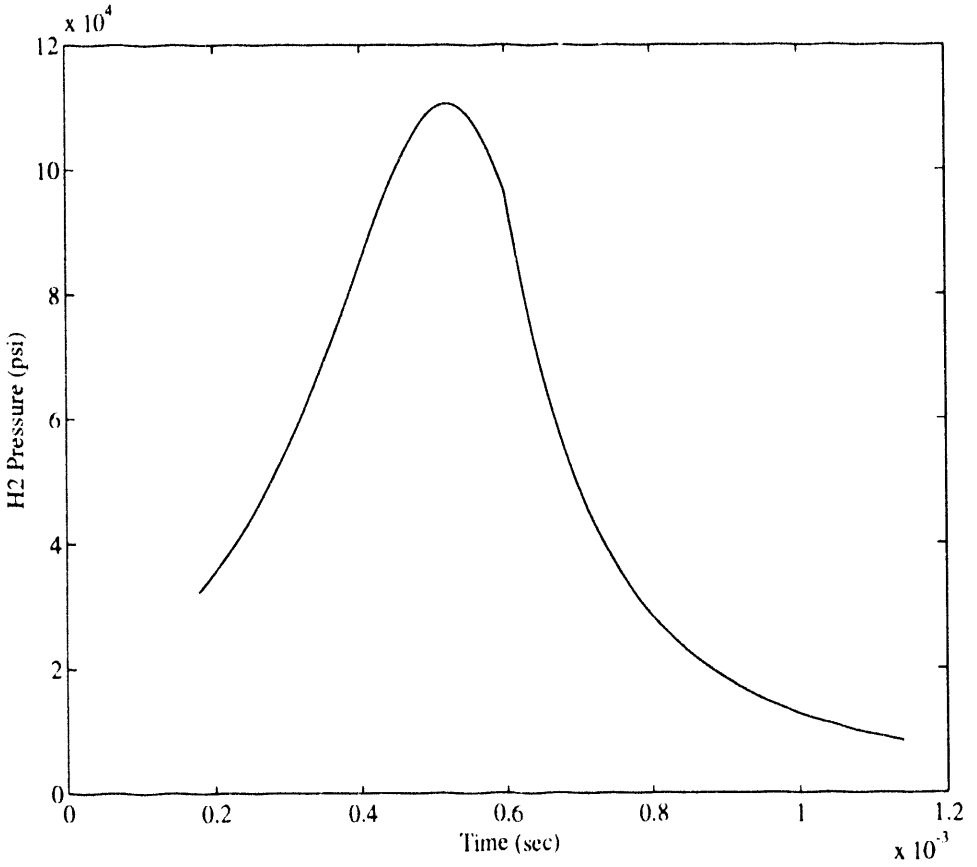

Figure 8. H_2 Pressure in Test 3

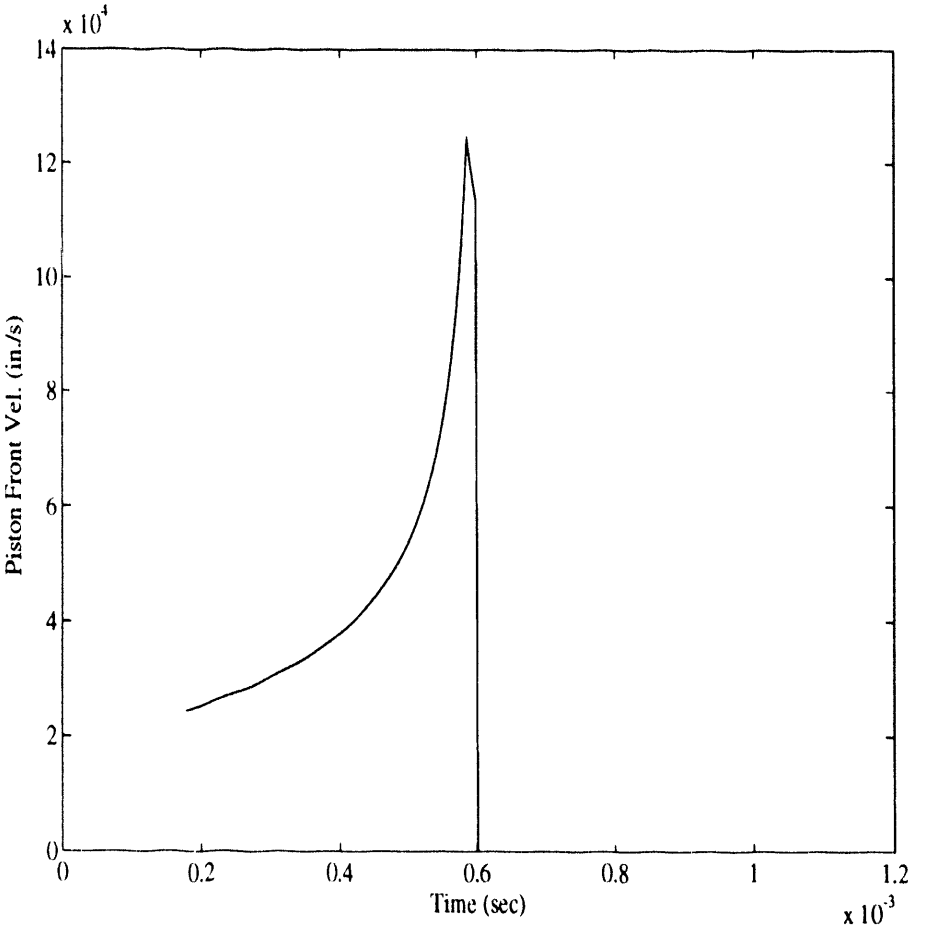

Figure 9. Piston Front Surface Velocity in Test 3

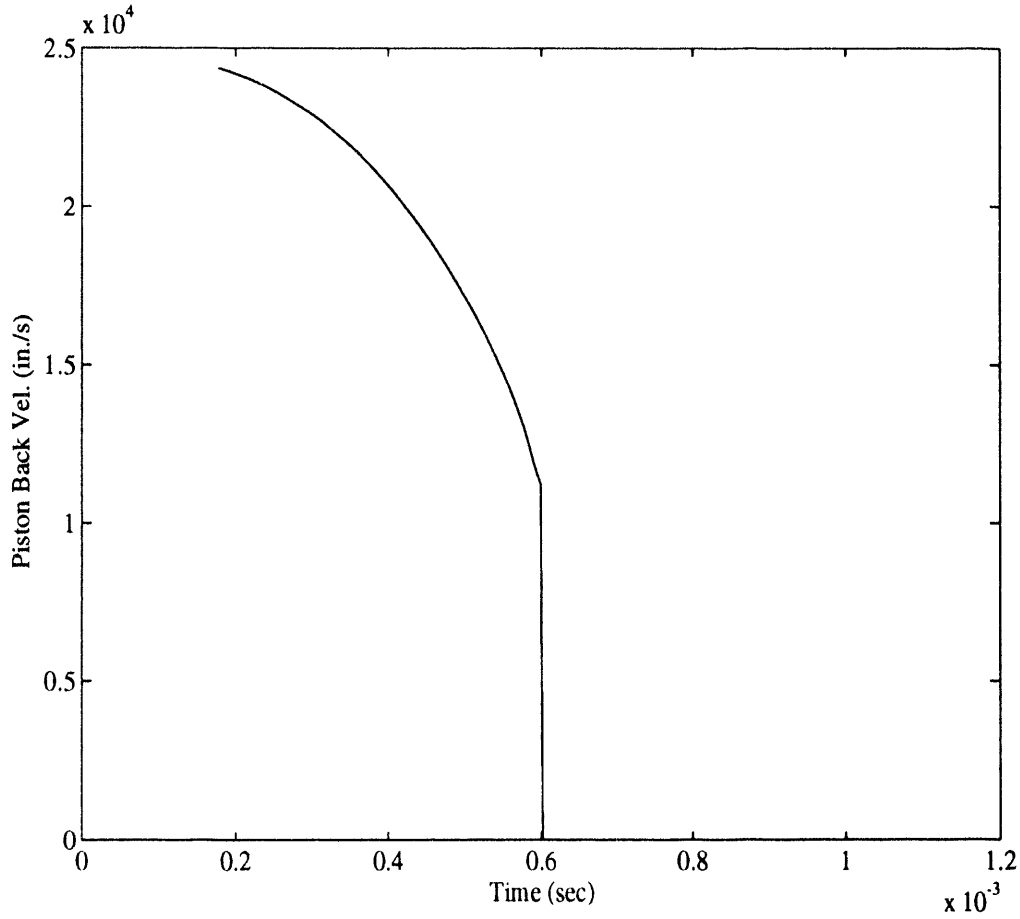

Figure 10. Piston Back Surface Velocity in Test 3

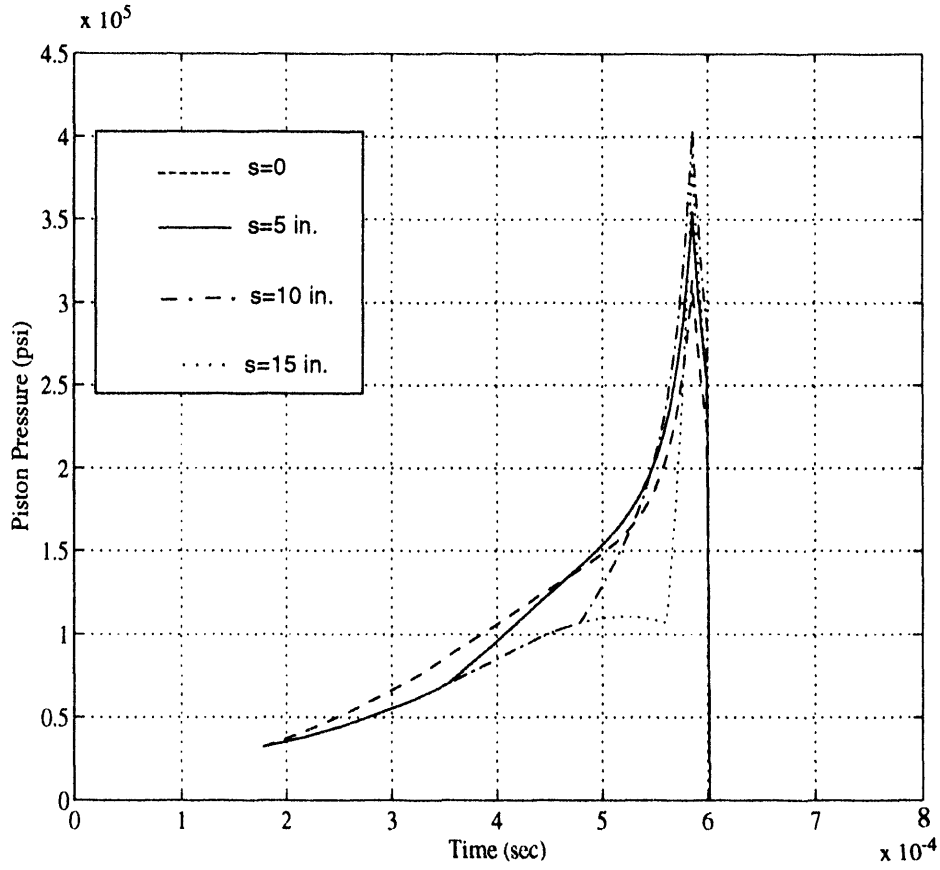

Figure 11. Pressure Histories at Several Axial Locations in the AR in Test 3

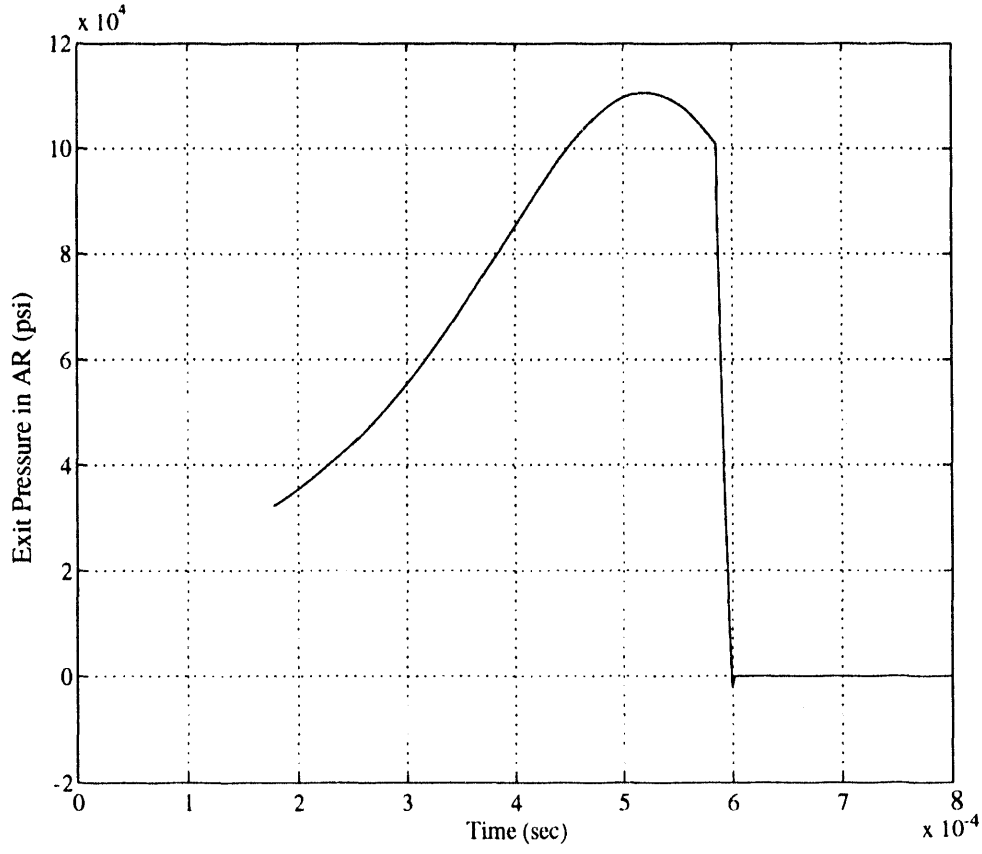

Figure 12. Pressure History at the Exit of the AR Tapered Region in Test 3

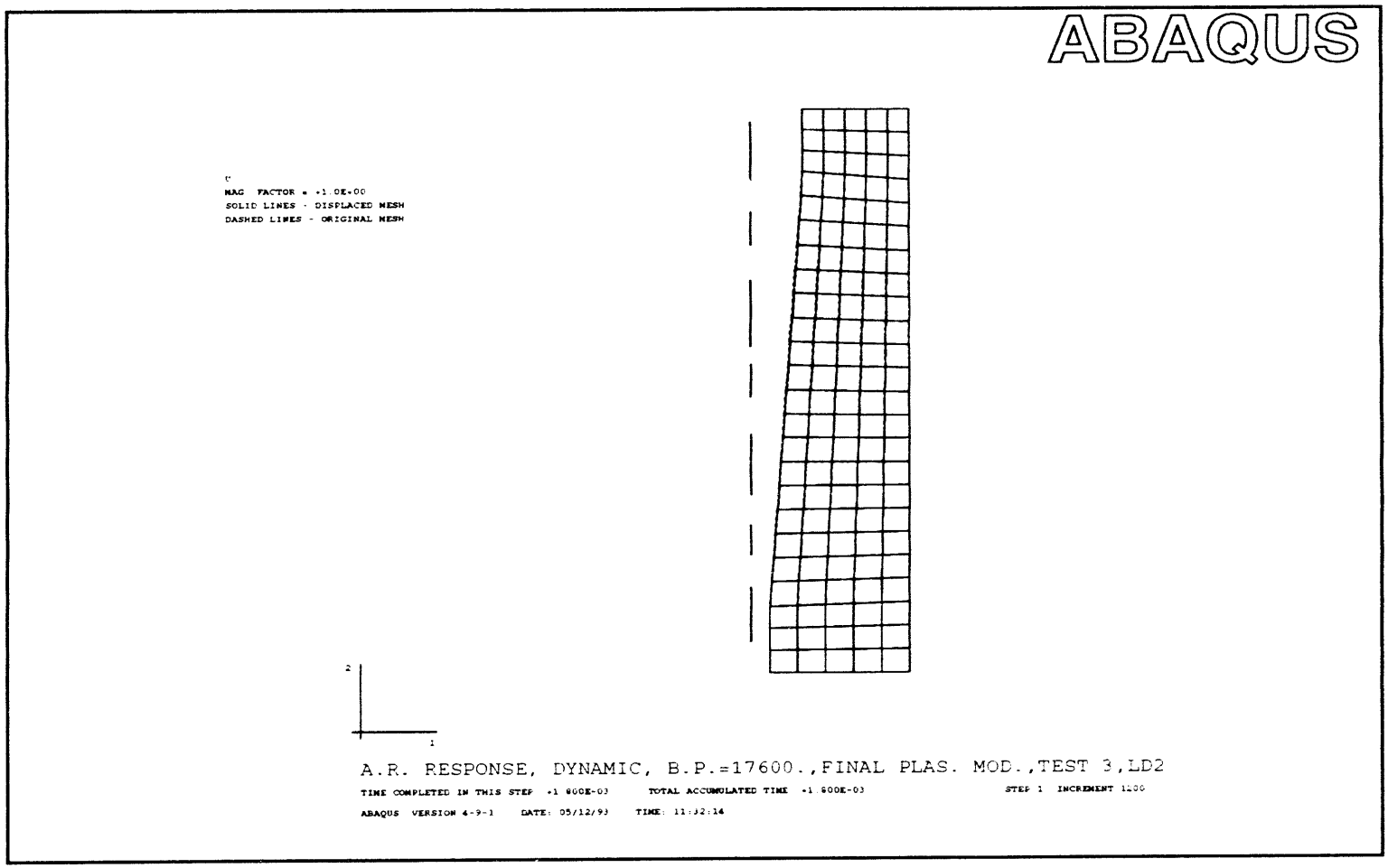

Figure 13. ABAQUS Structural Model of the AR

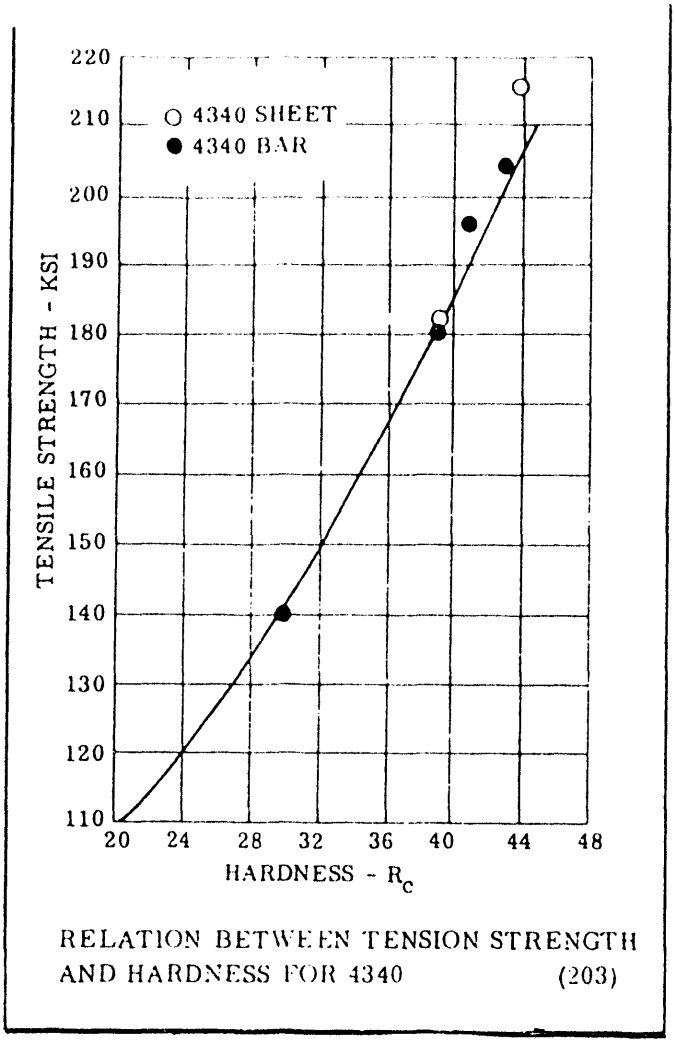

Figure 14. Tensile Strength of 4340 Steel versus Rockwell C Hardness

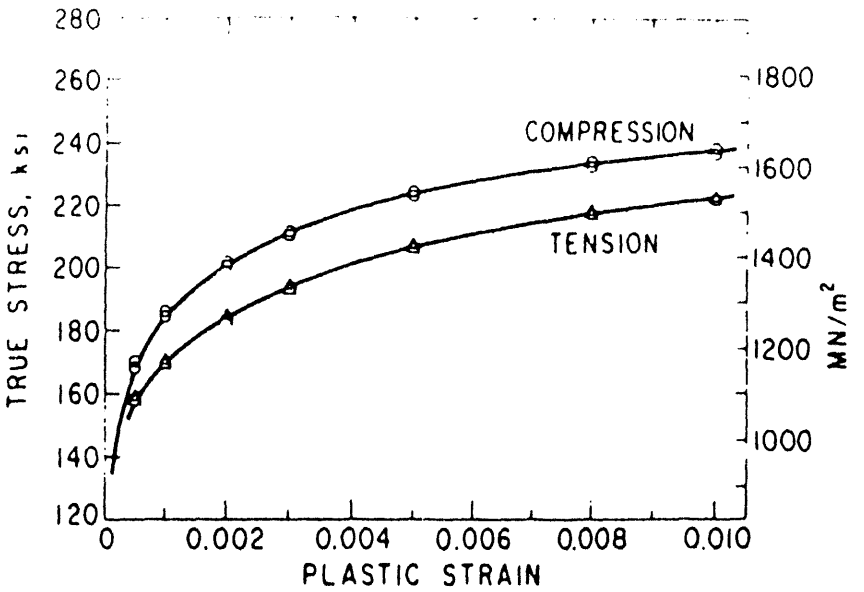

True stress-plastic strain curves in tension and in compression for lower bainite in AISI 4340 steel, transformed at 315 °C (588 °K) for 30 min. Tension-compression specimens.

Figure 15. Stress-Strain Curves of 4340 Steel in Tension and Compression

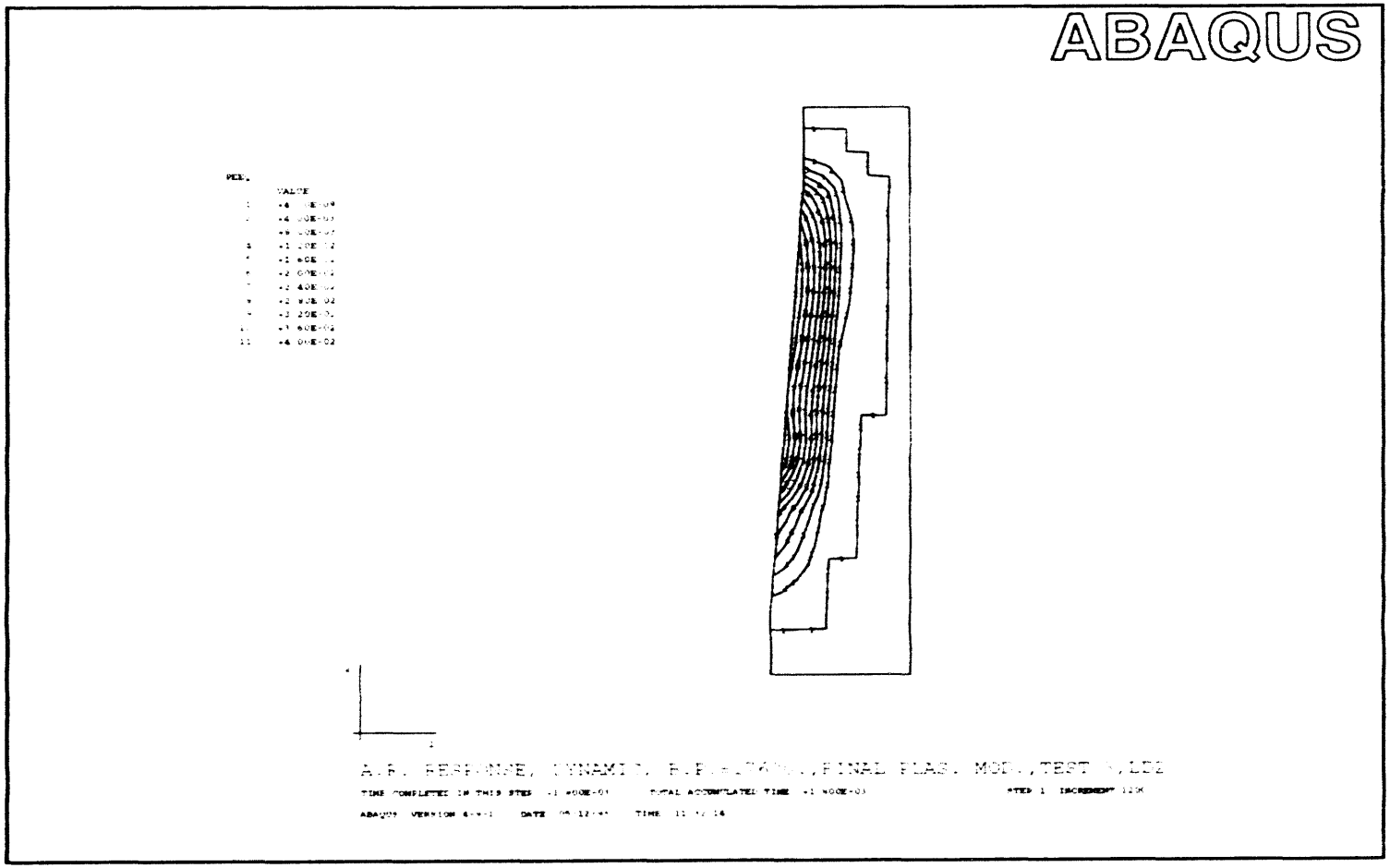

Figure 16. Equivalent Plastic Strain Contours in the AR After Test 3

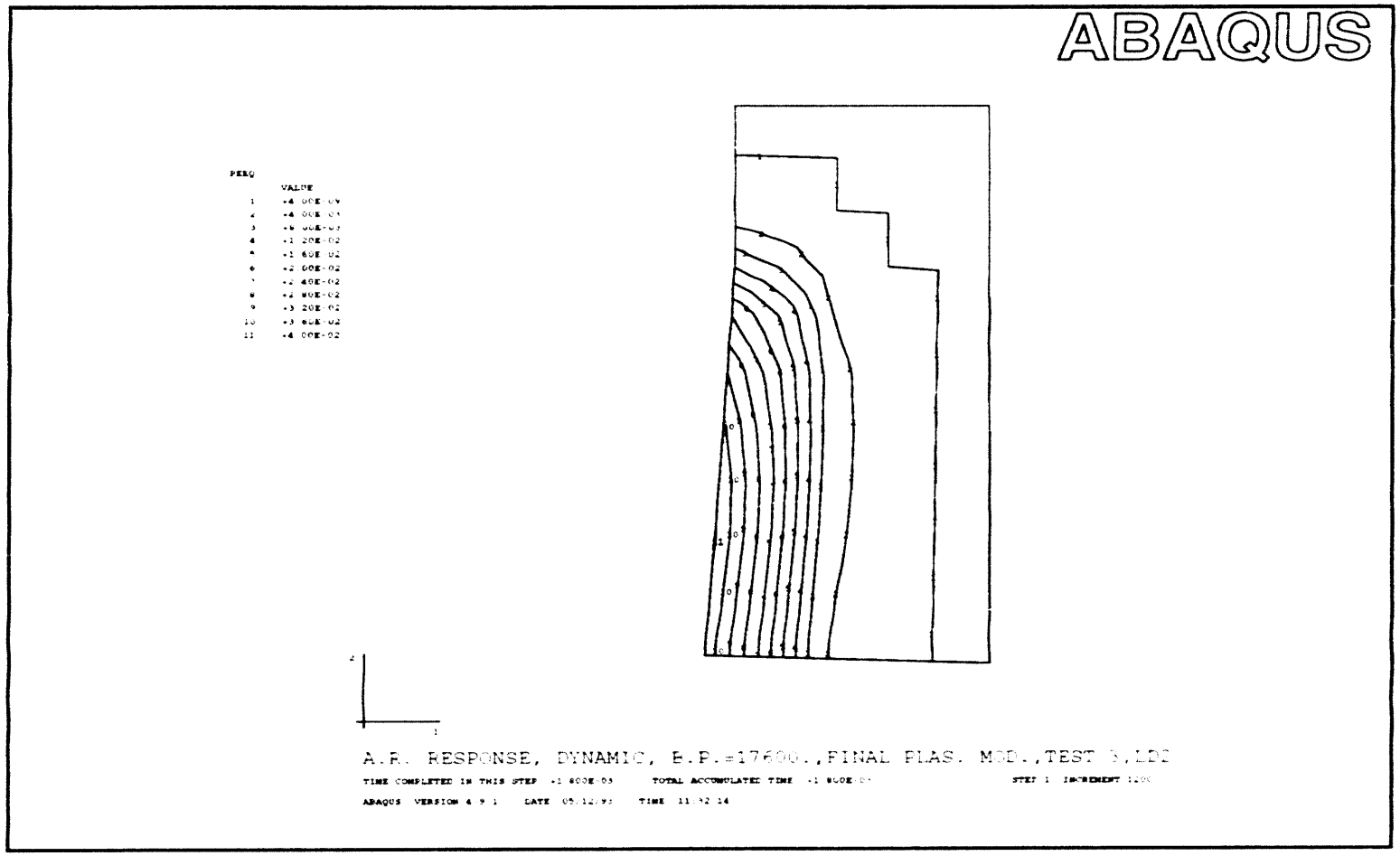

Figure 17. Detail of Contours with Highest Equivalent Plastic Strain

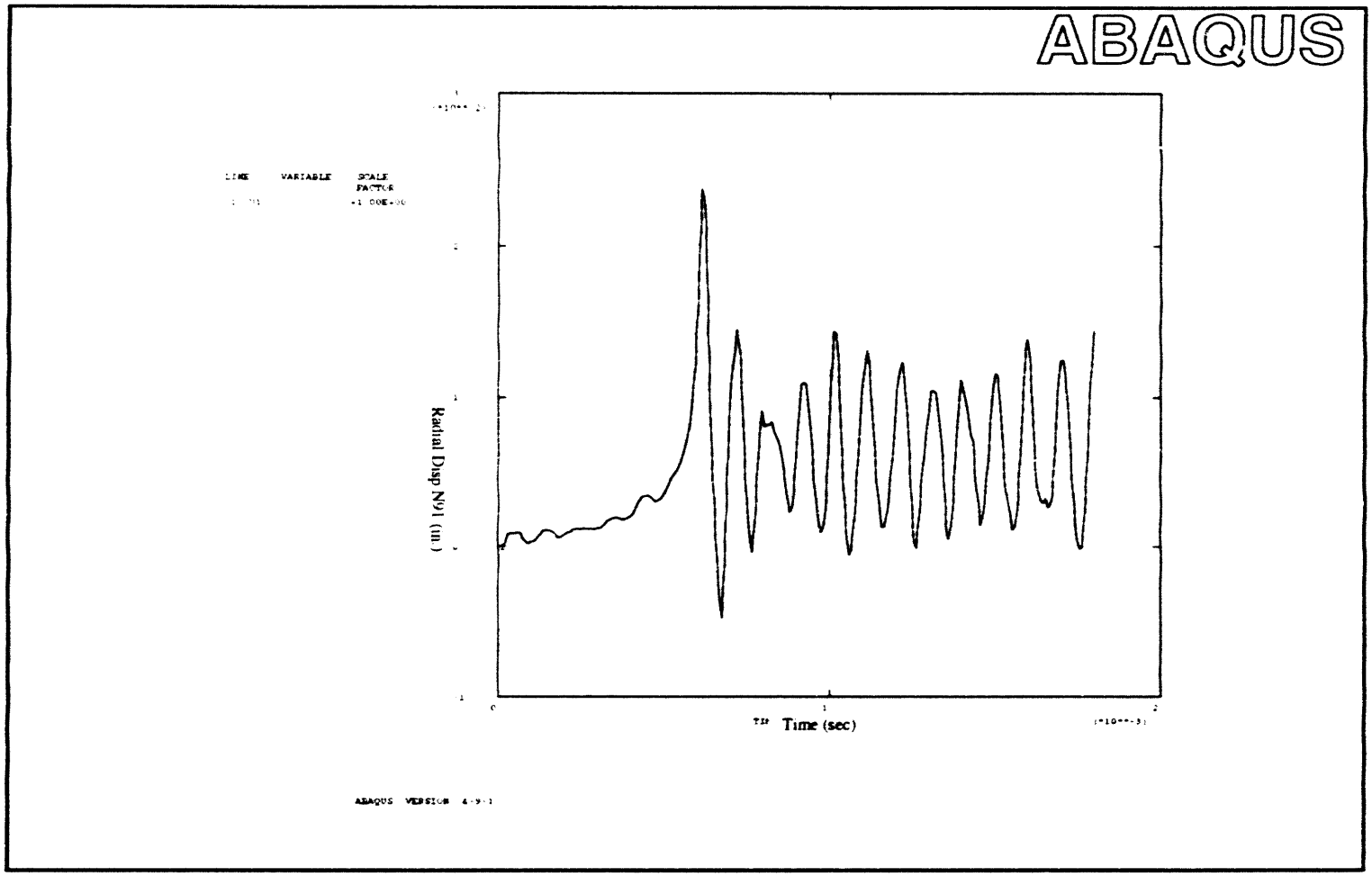

Figure 18. Maximum Radial Displacement at the Inside Surface of the AR in Test 3

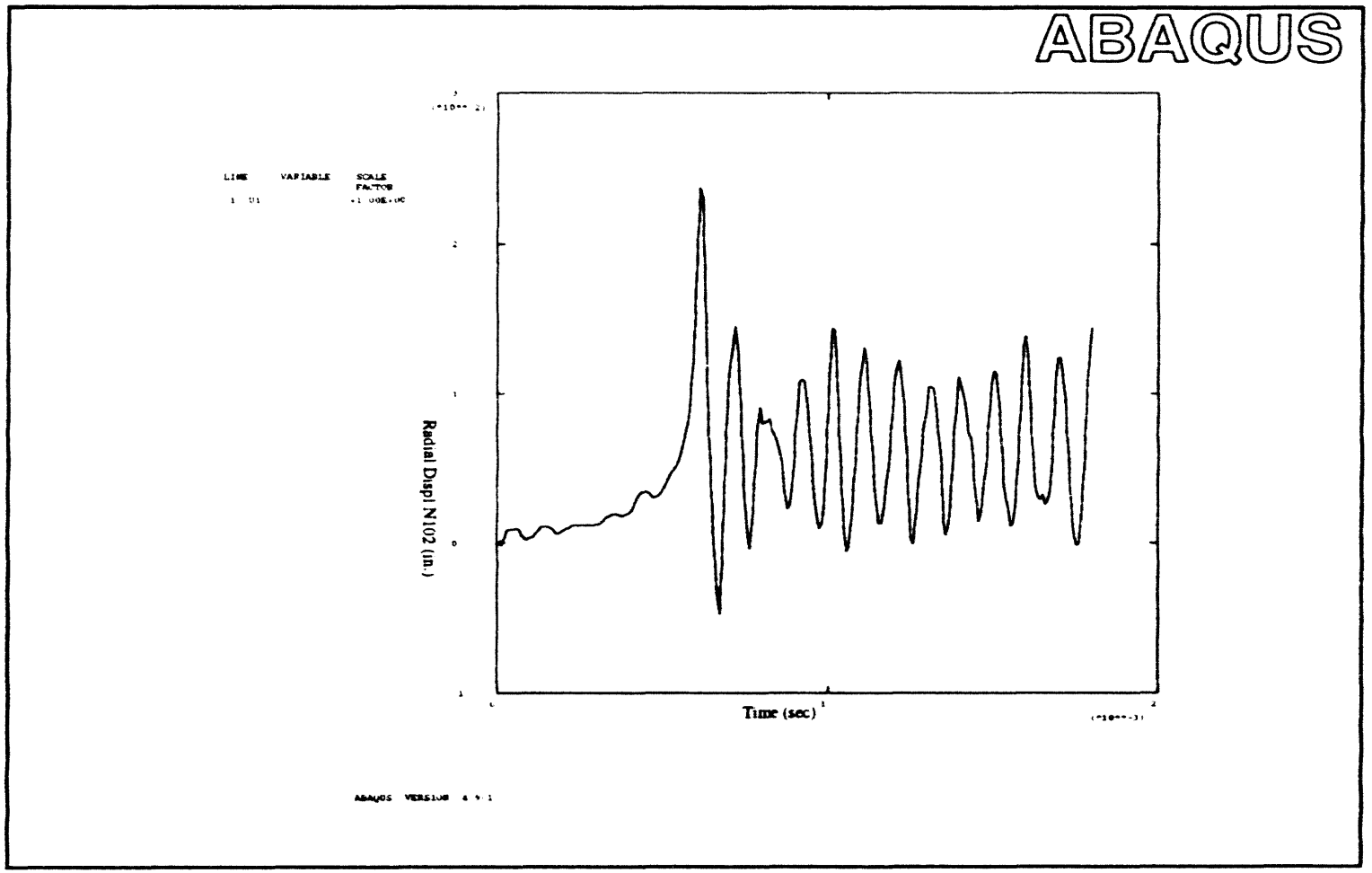

Figure 19. Maximum Radial Displacement at the Outside Surface of the AR in Test 3

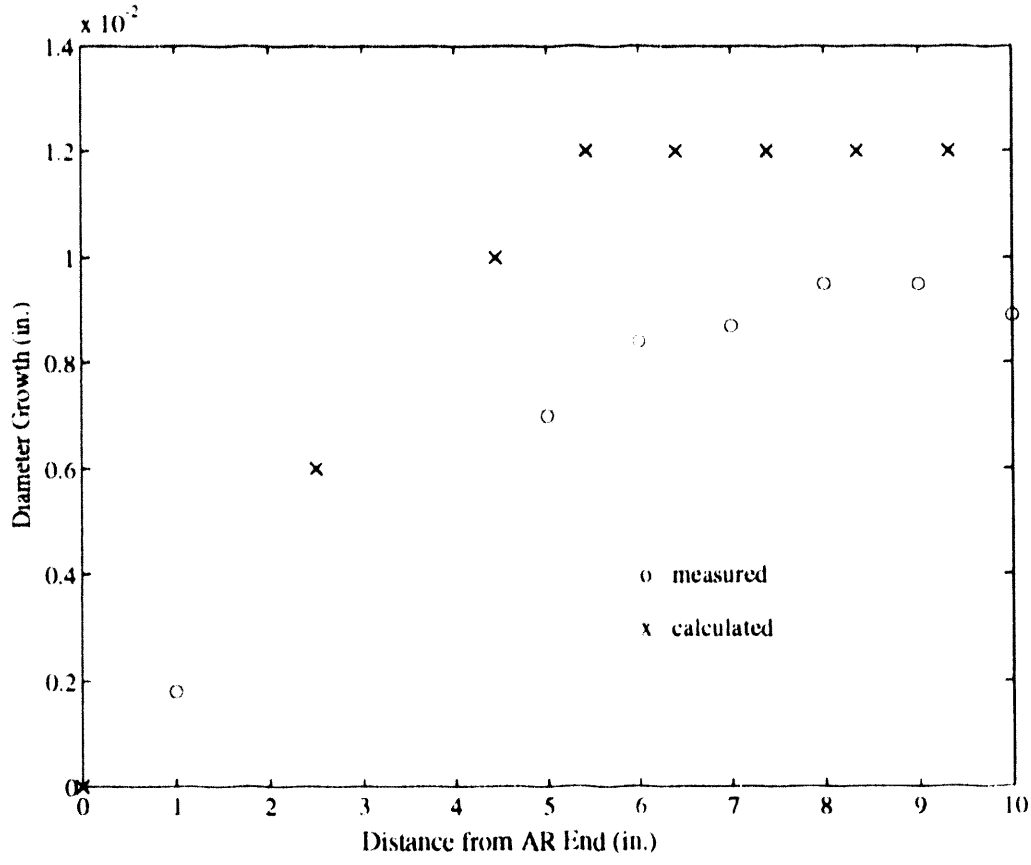

Figure 20. Measured and Calculated AR Outside Diameter Growth in Test 3

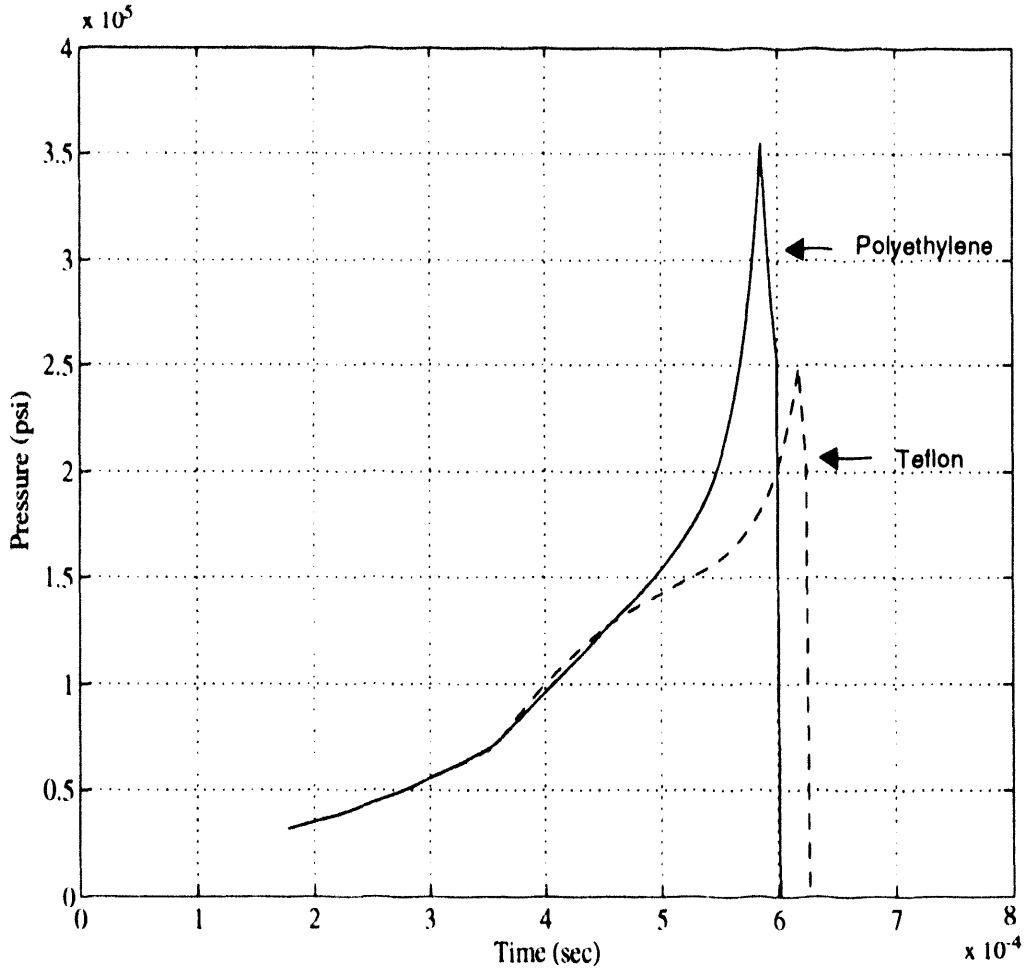

Figure 21. Pressures in the AR (s=5 in.) for Polyethylene and Teflon Pistons

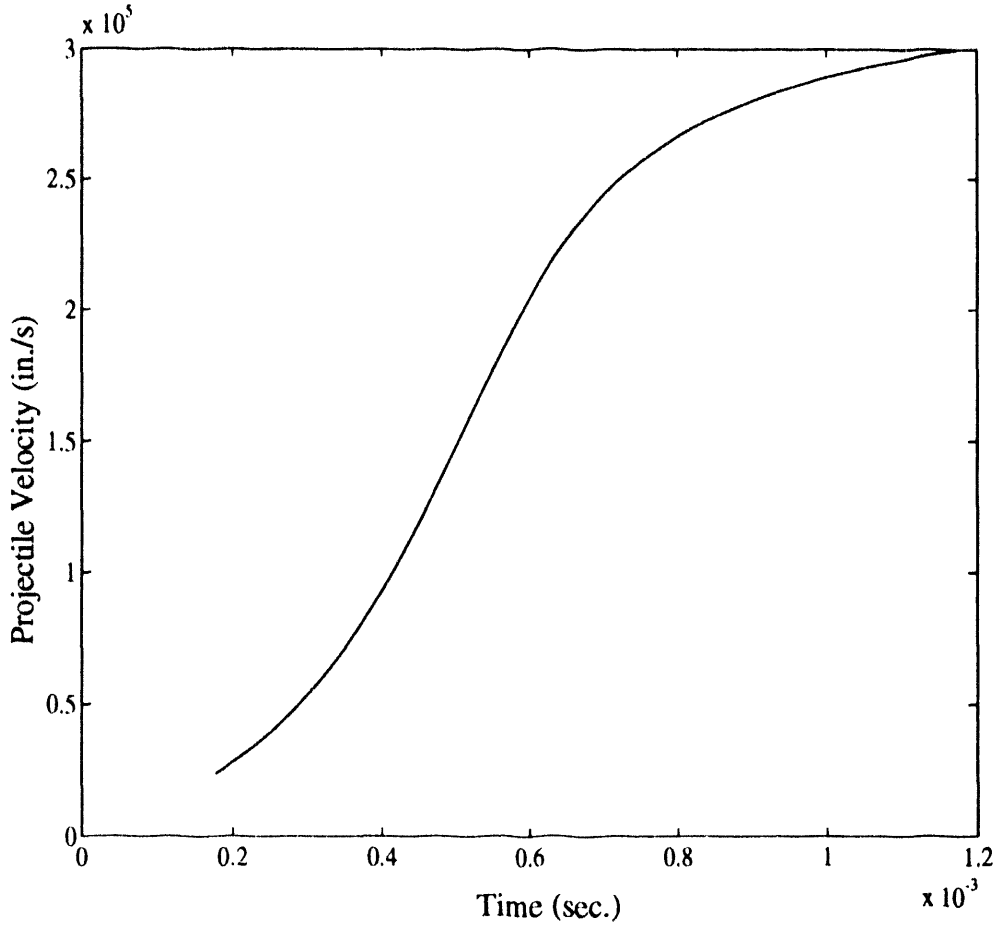

Figure 22. Velocity of the Projectile in Test 3 for Teflon Piston

Distribution:

S. J. Bless
Institute for Advanced Technology
4030-2 W. Braker Lane
Austin, TX 78759-5329

A.J. Piekutowski
Impact Physics Laboratory
University of Dayton Research Institute
300 College Park
Dayton, OH 45469-0180

Sandia Internal Distribution:

MS0439	1400	E.H. Barsis
MS0821	1433	P. L. Stanton
MS0821	1433	C. A. Hall
MS0821	1433	L. Chhabildes
MS0411	9823	M. J. Forrestal (3 copies)
MS0439	1434	D. R. Martinez
MS0439	1434	D. B. Longcope
MS0821	1433	M. Shahinpoor
MS0820	1432	F. Norwood
MS0821	1433	D. E. Grady
MS0899	7141	Technical Library (5 copies)
MS0619	7151	Technical Publications
MS0619	7151	Mabel Hurley (housekeeping)
MS0100	7613-2	Document Processing (10 copies) For DOE/OSTI

DATE

FILMED

7/7/94

END